Significant yield benefits from basalt soil amendments in the Southeastern US

Ella Milliken[1*], Liza Swanson[1], Rachel Gregg[1], Adam Wilbourne[2], Alex Woodley[3], Kenzo Esquivel[4], Noah Sokol[4], Jennifer Pett-Ridge[4], Noah Planavsky[1,5]

1. Earth & Planetary Sciences, Yale University, New Haven, CT, United States
2. Wilbourne Land and Timber, Clarksville, VA, 23927
3. Crop and Soil Sciences and NC Plant Sciences Initiative, North Carolina State University, Raleigh, NC
4. Physical and Life Science Directorate, Lawrence Livermore National Laboratory, Livermore, CA
5. Yale Center for Natural Carbon Capture, Yale University, New Haven, CT

*Corresponding Author: ella.milliken@yale.edu

Abstract

There is increasing evidence that carbon dioxide removal (CDR) strategies will play a significant role in global greenhouse gas management[1,2]. Enhanced weathering (EW) is a CDR strategy with substantial carbon removal potential, which can simultaneously offer agronomic and soil fertility co-benefits to farmers[3]. These co-benefits have been extensively theorized, but few agronomic field trials have quantified yield increases attributable to EW. In this study, we present substantial (>20%) yield benefits from a 2-year conventional corn-soy strip trial of basalt application in the Southeastern United States. Increases in soil pH and losses in total cation concentration in the upper portion of the soil provide evidence of basalt weathering. We also present stochastic economic analysis of net per-hectare revenue shift with subsidization of basalt purchase, hauling, and application. If rock application is subsidized, these results suggest a potential benefit to the grower of >$250 per-hectare for soybean production, and >$750 per-hectare for corn production within the first two years of application. This work provides some of the first direct evidence of 20% yield increases associated with EW in a large-scale strip trial, as well as substantial economic and agronomic benefits of EW on working lands.

Introduction

Limiting the most severe impacts of climate change will require substantial removal of carbon dioxide (CO_2) already accumulated in the atmosphere[4]. Despite international agreements and mitigation efforts, current national commitments remain insufficient to meet temperature targets[5]. Even under optimistic mitigation scenarios, pathways to meeting climate targets and achieving net-zero emissions rely on large-scale deployment of carbon dioxide removal (CDR) technologies to balance residual emissions[1]. As such, it is increasingly clear that large-scale CDR technology must be developed, invested in, and deployed at scale to meet long-term climate goals[2]. The scalability of a CDR strategy depends not only upon its technological feasibility; the cost, durability of carbon removal, and (perhaps most importantly) the social/economic incentives for adoption are also critical[6]. It has been commonly argued that the most successful CDR pathways will offer direct and tangible benefits to the systems and communities in which they are implemented, such that CDR alone is not the only driver for its deployment[7].

Within the next half-century, climate change will reshape farming communities and the agricultural industry around the world[8,9]. Climate change is predicted to significantly reduce crop yields in the world's most productive agricultural regions, driven by increasing extreme droughts and storms, altered pest and disease patterns, and high summer temperatures altering local water availability during the growing season[8,10–14]. Fertilizer and amendment costs remain highly volatile, driven in part by fluctuations in energy costs. At the same time, farmland is being rented at unprecedented rates, reducing the share of agricultural profits retained by farming communities[15,16]. These economic pressures may discourage investment in management practices that require long-term returns, particularly on rented land[17–19]. As agricultural communities adapt to both climatic and economic shifts, there will be increasing interest in CDR approaches that can improve soil health, enhance crop performance and resilience, while reducing input costs[20,21].

Enhanced weathering (EW) has emerged as one such CDR approach, with the potential to improve agronomic outcomes while providing a significant supply of CO_2 removal[3,22]. The aim of EW is to accelerate chemical weathering by moving fine-grained, reactive, cation-bearing rocks (e.g., industrially milled basalt) into settings with high water fluxes and high CO_2 concentrations. Most work has focused on application of crushed rock to agricultural fields using existing infrastructure. As these feedstocks dissolve, the release of cations (e.g. Mg^{2+} or Ca^{2+}) is charge-balanced by the conversion of CO_2 to bicarbonate (HCO_3^-)[23]. These coupled weathering products can either be retained in soils and groundwaters, or travel through watersheds into oceans, where they can be permanently stored on millennial timescales.

Low soil pH, increasingly driven by persistent nitrogen fertilizer use, is a pervasive issue across agricultural communities that reduces nutrient use efficiency and lower crop yields[24,25]. By supplying nutrients and ameliorating soil acidity, EW may provide agronomic benefits to farming communities that create strong incentives for adoption. Additionally, basalt EW may increase bioavailable micronutrients while improving physical soil structure and water-holding capacity, providing multiple pathways to enhanced crop yields. If the costs of basalt purchase and application are offset through carbon markets or government subsidies, these agronomic benefits could be realized with substantially lower financial risk, improving both farm profitability and resilience.

The potential agronomic benefits from silicate addition have been extensively theorized; however, direct documentation of these effects has lagged. Though the literature is expanding, evidence for the agronomic and soil fertility co-benefits of basalt EW under true field conditions on working farms is still limited[26–31]. While the effect of increased soil pH has a proven relationship with yield[32], there has been little research demonstrating that applied silicates dissolve significantly and rapidly enough to produce measurable soil and crop responses within the first few growing seasons after application.

Here, we show some of the first evidence in a large-scale strip trial that basalt application can substantially impact yields by 20-35%. Further, we directly quantify the financial benefit for farmers through a coupled economic analysis of the expected net revenue gains for famers. We find that there is the potential for large financial benefits to farmers if the practice is subsidized. We report results from repeated soil testing and crop yield measurements across two growing seasons after basalt application. By providing field-based evidence of rapid and meaningful agronomic responses to EW, we demonstrate that EW can deliver tangible near-term benefits to farmers alongside longer-term climate mitigation, strengthening the case for its scaling potential.

Results and Discussion

We applied 44.8 t ha^{-1} of fine basalt to an area of 0.88 ha in 3 strips, which were paired with unamended control plots (see Fig. 1 for experimental design and SI Table 2, Fig. 4 for crushed basalt composition). We took soil samples at 5 timepoints: a baseline prior to basalt application (BL), a post-deployment sample (R0), post-soy harvest, approximately six months after application (R1), pre-corn planting (R2), and post-corn harvest, approximately 1.5 years after application (R3). We measured the effect of basalt on soil pH 3 times over 2 years in comparison to the baseline (R1, R2, R3 sampling timepoints) and effects on soy and corn crop yield at the end of each growing season.

There were significantly higher yields in both soybean and corn seasons in basalt-applied strips relative to unamended control plots, increasing by 22.92 ± 15.3 % and 36.50 ± 9.83 %, respectively ($p<0.0001$) (Fig 2a-b). This clear impact of basalt application on yield is high in comparison to other reported yield changes, though Jordan et al. (2026) finds similar magnitudes of increase in rice paddies in India[26–30]. This is partially a function of high application rates of basalt in this study, such that there is an increase in bulk addition of cations and nutrients, as well as relatively rapid dissolution. To the best of our knowledge, the boost in corn yield under crushed basalt application is the most pronounced agronomic benefit from crushed basalt application recorded in the literature[26–30].

Soil pH trends were consistent with yield increases in plots with crushed basalt. Interpolations of pH over the field show clear increases in the basalt-treated pre-corn planting (R2) timepoint, as well as the post-harvest (R3) timepoint (Fig 3). At the baseline (BL) timepoint, there are clear differences in soil pH across the east-west transect of the field; the western portion tends to be quite acidic, with pH values ranging from 5.5-5.9. On the eastern portion, pH is higher with a range of 5.9-6.3. At the resample timepoint R2, clear differences are illustrated in regions recovering from soybean planting. In basalt applied sections, pH remains in the 5.9-6.6 range, with some hotspots of acidity. In contrast, the control areas saw a larger decline towards pH values of 4.9-5.8.

These increases are accompanied by clear evidence of a basalt weathering rate, or dissolution rate, determined through the measurement of total cation loss from the soil. The determination of weathering rate showed a 24.64 ± 5.64% cation accounting rate (c.f.[26,27,33]; see methods) and a Titanium (Ti)-adjusted rate of 22.1 ± 6.23 % after 6 months in basalt-treated areas, with no significant shift in the cation content controls (Fig 2c; SI Fig 3). This dissolution does not remove exchangeable cations prior to digestion, which likely renders it conservative. The reported dissolution rates are within the range previously published estimates from subtropical environments, where relatively high temperature and precipitation regimes cause accelerated rates of removal compares to more temperate environments[27,34–37].

The exact mechanism driving this yield increase is difficult to completely isolate. We see clear pH shifts from basalt application at the R2 timepoint; however, it is unlikely for pH alone to cause such a clear shift in yield, as pH generally stays above 5.8 in the first year, which is within the optimal corn/soy range in this region[38]. The basalt applied is rich in trace micronutrients, such as Ca, Mg, Zn, Cu, Si, and Mn, which many farmers traditionally only apply in micronutrient fertilizer mixes (SI Table 2). Additionally, given the high fraction of Si in the basalt, and clear increases in corn yield relative to soy, bioavailable Si may be playing a strong role in this system. It is important for future work to isolate the mixed effects of micronutrients, specifically bioavailable silica, from pH shifts due to basalt.

The background soil characteristics of this study area (see SI Fig 1) make it likely to significantly benefit from EW application. The baseline cation exchange capacity (CEC; see methods) within the field is quite low (<8 milli-eq/100g), with relatively low base saturation (<60% below 4 cm in the A horizon). These soils are also highly degraded from decades of historic tobacco farming, which is well-documented to cause significant declines in soil fertility over time[39,40]. As such, there is a low availability of bioavailable cations within the field, consistent with soil properties throughout the Southern Piedmont region[41,42]. This deficiency will not only lead to a low buffer capacity due to large shifts in local acidity, which will decrease crop performance, but will lead to relatively reduced climate resilience over time[43].

There are a few major weather phenomena seen through the course of this field trial which may influence these yield differences. In June-July 2024, the entire region experienced a significant drought, with no major rains over the 2 months of early soybean growth. In August 2024, Hurricane Helene swept through the region, leading to significant flooding and subsequent potential anoxia in crop roots. There may be two converse impacts from basalt addition that could allow for increased resilience in this study. First, the yield could be driven in part by increased water retention within the field, given that there was a significant drought in the first year of the trial. Basalt amendments will increase the fine particle size content of sandy soils, potentially increasing the physical capacity of the soil to retain water. The upper portion of these soils are sandy; thus, the incorporation of the fine basalt shifted the particle size distribution (SI Fig. 3). This observation raises the need for future work on how basalt addition may change to hydraulic soil properties in soils with low water holding capacity. The increased aboveground yield from the soybeans is likely to be matched by increased root growth[44–46]. This growth may allow for increased resilience during wet, high saturation periods by increasing access to pore spaces containing oxygen.

Early in the corn season (April-May 2025), there were uncharacteristically high rates of precipitation leading to remarkable growth of the young corn. Following this, June and July 2025 saw comparably little precipitation, leading to significant late-season drought conditions. Increased early growth due to more favorable pH values and micronutrient addition from basalt application may have allowed the corn to remain more resilient during the prolonged stress period in comparison to controls. The abnormal precipitation regimes seen in these two years are becoming increasingly prevalent with climate change, as weather patterns become increasingly volatile with altered patterns of heat redistribution[47,48]. Our findings suggest that the addition of basalt may aid in maintaining crop health through variable weather patterns, ultimately building localized climatic resilience.

A stochastic economic analysis of corn-soy sales and amendment costs (see methods) demonstrated a clear increase in revenue with the inclusion of subsidization of the basalt amendment for the first year. With mild subsidization of the basalt (0-10%), soy showed an averaged loss over the first year of $683.01 per hectare, while corn showed an average loss of $233.27 per hectare. With moderate to high subsidization, soy showed a loss of $164.56 per hectare in the first year, while corn showed an averaged gain of $295.18 per hectare. With full subsidization for the first year, soy showed a gain of $296.76 per hectare, and corn showed a gain of $756.49 per hectare. Expected soy revenue gains remained below expected gains from corn across scenarios, consistent with lower per-hectare yield and revenue increases. These monetary increases are quite significant; given that, in 2020, average gross production value of corn was approximately $1730 per hectare, and the gross production value of soy was approximately $1230 per hectare, with the net production value of both crops hovering around $0[49]. The average per-hectare cost of applying basalt was \$419 ± 153.65; given average values across all Monte Carlo values, the 1-year yield gain needed to break even, with no subsidization, is 54.69% for corn and 85.15% for soy. For a full payback in 2 years, the per-year yield gain must be 27.34% for corn and 42.58% soy. For a 5-year payback period, the per-year yield gain must be 10.94% for corn and 17.33% for soy. These values are largely within the values shown by this trial and other experimental works[26–30]. We note that the yield gains used as inputs to this simulation are derived from a single site with historically degraded soils and low cation exchange capacity, conditions that likely favor above-average agronomic response to basalt application. Revenue projections should therefore be interpreted as indicative of outcomes on similarly responsive soils. Nevertheless, it is apparent that, with the use of subsidies or maintenance of voluntary carbon market structures, these per-hectare gains have the potential to significantly improve agricultural outcomes in Southeastern US farms.

The presented results in this study provide motivation for additional work on the agronomic benefits of EW on working farms. This work suggests that the US Southeast may be a prime region for the development of large-scale EW deployments. Not only do high dissolution rates in the first several years ensure carbon drawdown through weathering, but we also expect to have clear, significant agronomic benefits through the introduction of micronutrients and pH shifts. This impact, will, if subsidized by carbon markets or included in national agricultural subsidies, directly lead to increased revenue for farmers. However, given that there are still clear profitable scenarios with no subsidization, this practice could be adopted by growers for the yield benefits alone.

The pronounced agronomic benefits in the Southeastern US provide additional strong motivation for additional field trials and basic research on the mechanisms behind the benefits of basalt soil amendments, such as micronutrient addition, water holding capacity, biologic effects, and soil structure.

Acknowledgements

The authors thank Wilbourne Farms, including farm operators Kade and Austin Wilbourne, for their continued support of this work. We also thank Lithos Carbon in their help in spreading and deployment logistics. NJP acknowledges support from Microsoft, the Yale Center for Natural Carbon Capture, and Foundation for Science and Technology. Work at LLNL was funded by the LLNL LDRD Program [24-SI-002] and supported by LLNL's 'Terraforming Soil' Energy Earthshot Research Center (EERC), funded by the U.S. Department of Energy Office of Science [Award# SCW1841]. Work at LLNL was performed under the auspices of the DOE [Contract DE-AC52-07NA27344].

Figures

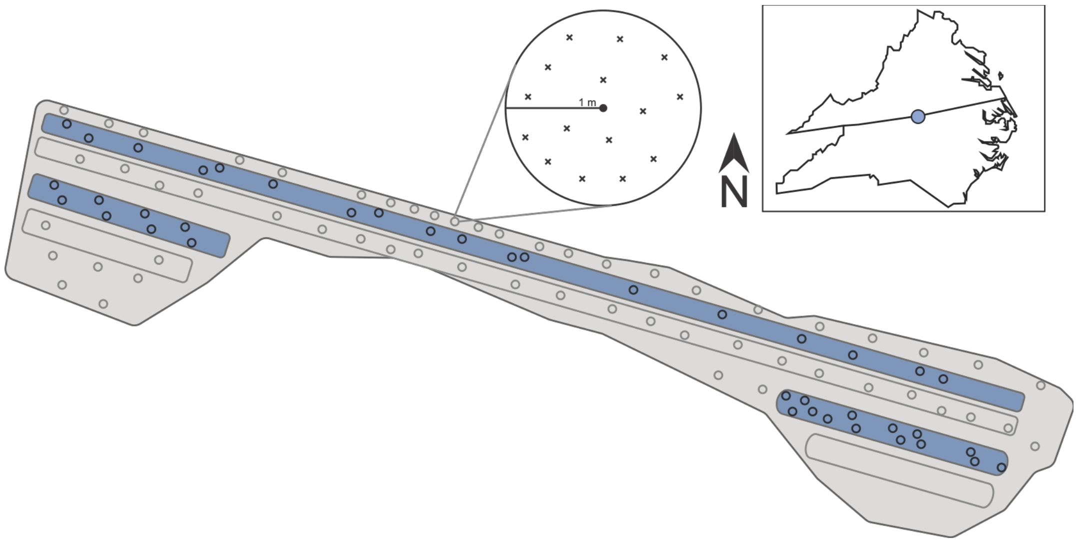

Figure 1. Field, application, and sampling pattern for study site in Clarksville, VA. The total parcel is 7.96 ha, with 0.88 ha applied (shown in blue), and 0.83 control ha set for harvest next door (outlined in grey). Samples were taken in the center of the applied rows, with 39 samples in basalt-applied areas, and 63 samples in control areas (all soil samples taken shown in circles). Only yield results from the outlined control areas are included in presented analysis. Soil sampling design is also shown for geolocated points; 15 composite points, taken to 15 cm depth, are collected from within a 1m radius of a given point, and composited for a given sample.

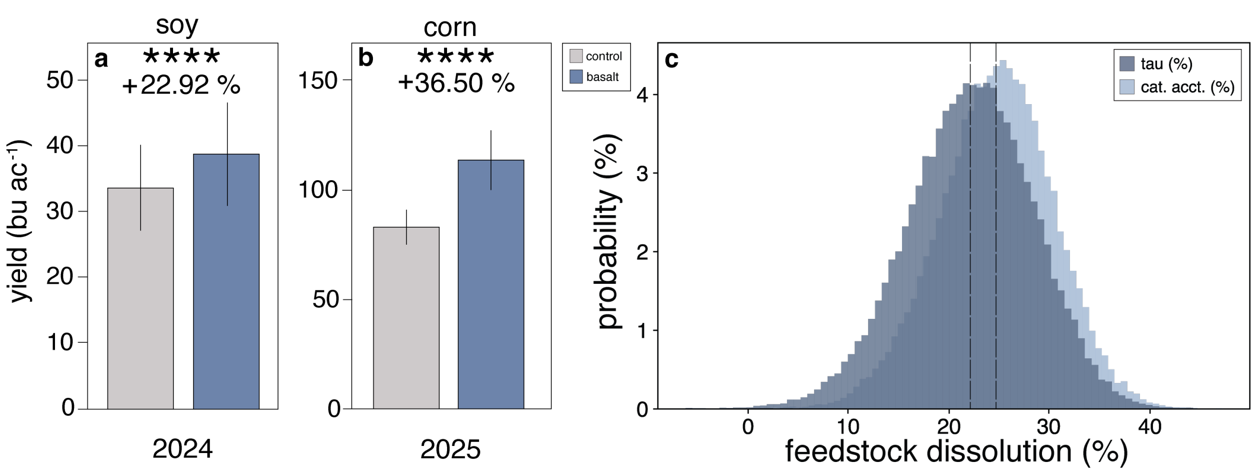

Figure 2. Yield of soybean and corn in basalt and control regions from 2 growing seasons post-application, and year 2 dissolution rate. a-b) Basalt yield is shown in blue, and control yield is shown in gray. Percent increase in the basalt yields as compared to the control areas is shown. Vertical bars represent the area-normalized standard error of the mean for each sampled strip. * = $p < 0.0001$. c) Full bootstrapped cation-equivalence from baseline (BL), post-deployment of basalt (R0), and resampling after year 2 corn harvest (R3) for both basalt and control regions is shown, with basalt timepoints shown in shades of blue and control timepoints shown in shades of gray.

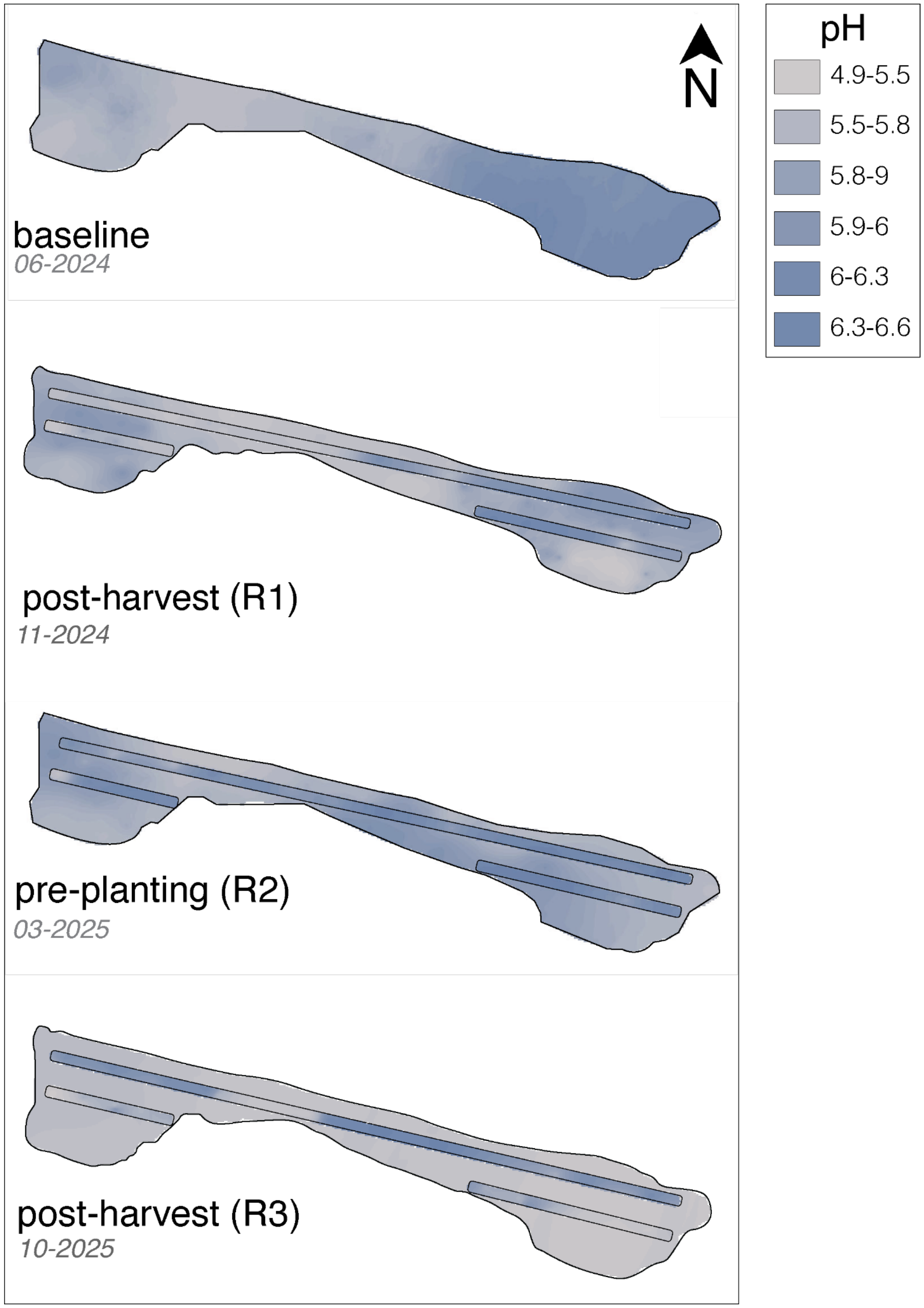

Figure 3. Interpolated changes in soil pH with and without basalt application at resampling timepoints. 39 basalt and 63 control samples were taken prior to basalt application (BL), after soy harvest (R1), before corn planting (R2), and following corn harvest (R3). Soil pH is binned between 0.1 to 0.6 pH units, depending on the frequency of a given bin. Soils show a baseline clear pH pattern over the entire field, with more acidic conditions seen on the western portion of the field and more neutral conditions seen on the eastern portion of the field. Clear increases are seen within applied rows in comparison to the control within the R2 and R3 period.

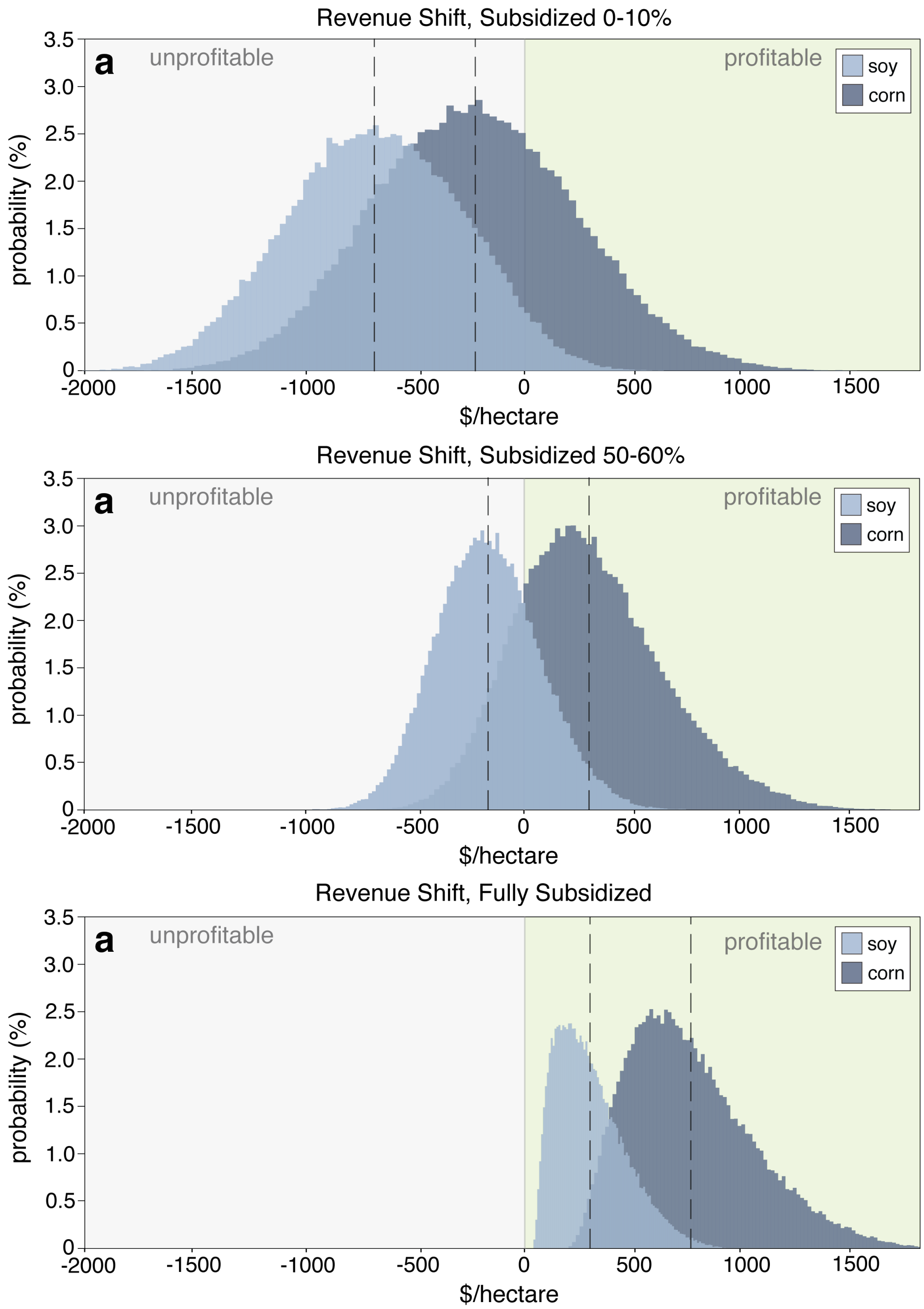

Figure 4. Monte Carlo simulations of expected per-hectare revenue shift for corn and soy with empirical yield gains for varying subsidization scenarios: a) subsidized between 0-10%, b) subsidized between 50-60%, or c) fully subsidized. Simulations included variable crop futures, base yields and yield increases, acreage, trucking efficiency, fuel costs, and % subsidization. 100000 simulations were run, and the probability of a given revenue shift outcome is shown on the y-axis. Means for each crop in each scenario are shown with vertical dashed lines. Unprofitable scenarios are colored in gray, and profitable scenarios are colored in green.

Methods

Site Description

The strip-applied field, totaling 7.96 ha, is located on a reduced-till corn-wheat-soybean agricultural farm in Clarksville, VA, in the Piedmont region of Southside Virginia (36.66, -78.48). This field has been in agronomic use for at least 60 years and was most recently transitioned from tobacco production to a corn-wheat-soybean rotation in 2012. The farm observes modified tilling practices for the region, with deep tilling once every 5 years, and ripping soils approximately every 5 years. The field was disked to 2 inches in June 2024 and March 2025. This field is only rain-fed, with no irrigation occurring in the past 10 years.

The soil across the study region is a fine, mixed, subactive, thermic, oxyaquatic hapludult, with a parent material of alluvial capped felsic granite. The Ap horizon continues to 22 cm, followed by an E horizon to 40 cm, and various B horizons continuing to 130+ cm (SI Fig.1). Soils are homogenous across the study region, with 0-2% slope over the area. Soil properties (pH, CEC, BS (%)) through the profile are shown in SI Fig. 1. Site temperatures were relatively consistent over multiple growing seasons, including prior to deployments (SI Fig. 2). Precipitation in 2024 and 2025 were more inconsistent than 2023, with drought conditions in June – July 2024, Hurricane Helene in August 2024, and a large drought In August 2025.

Agronomic Applications

Following winter wheat harvest in June 2024, basalt was applied in 3 strips over the study region, each with a width of 40 ft, with lengths of 1568 ft, 315 ft, and 490 ft respectively for basalt strips, and 1590 ft, 250 ft, and 381 ft respectively for control strips. totaling 0.88 ha at an application rate of 45.7 dry metric tons ha^{-1} at 18% moisture (Fig. 1). Physiochemical characteristics of the feedstock are described in the supplementary information (SI Table 2, SI Fig, 4). The rest of the field remained as control regions. The field was planted with soybeans at a density of 395,200 seeds/ha on June 17, 2025. The field was treated equally with 5.6 kg ha^{-1} of Micromix at planting containing boron, zinc, copper, molybdenum, and manganese in May 2025, along with 6 N-30 P-30 K at 252.19 kg ha^{-1} shortly after planting. Following soybean harvest in late October 2024, rye cover crop was immediately applied. In March 2025, the field was rip-tilled at 30 cm, the rye cover crop was sprayed with Round-up, and poultry litter was applied at 3.9 metric tons ha^{-1}, with a mean N concentration of 11.1 ± 4.0 kg per ton. In April 2025, 3 weeks after rye desiccation, corn was planted at a density of 61,750 seeds ha^{-1} with 7.41 gallons ha^{-1} in-furrow of Riser Pro. After planting, dry fertilizer was applied with a 14 N-7 P- 29 K-4 S at 410 kg ha^{-1}, as well as 5.6 kg ha^{-1} of Micromix, containing boron, zinc, copper, molybdenum, and manganese in May 2025. 3 weeks after planting, liquid N (24 N-0 P-0K-3S) was applied at 320 lbs ac^{-1}, for a total applied rate of approximately 225 kg ha^{-1} of N in 2025.

Yield Measurement

At time of normal harvest, the soybeans and corn in the 3 basalt applied strips were harvested down the center of the applied area with a 30 ft combine head. A 10 ft buffer was left between the basalt strip border and control harvest areas, and the untreated crop grown next to the basalt was harvested in strips. The Climesmart FieldView GPS system was used to approximate the total length of area harvested to calculate yield for each treatment. The total mass of grain from each applied region was weighed with a Meridian Seed Tender with built-in scales. The total area harvested for both control and basalt regions was calculated and weighted by area to give a total yield for both basalt and control treatments. Error in percent increase is reported as standard error of the mean.

Soil Analysis

For the basalt-applied region and the control-applied region, baseline samples (BL) were taken prior to and following application (R0) to 15 cm with 39 basalt sampling points and 63 control sampling points. (Fig. 1). R0 samples are only used for weathering rate calculation. Each sample taken is a composite of 15 individual cores, taken within a meter radius of a preset geolocated point with a 1 in accuracy, collected with a drill auger bit to 15 cm depth. 102 soil samples were then taken at the same preset points following soybean harvest (R1), prior to poultry litter application (R2), and following corn harvest (R3). Soils were dried at 60°C, sieved to 2 mm, and ground at Waypoint Analytical Labs in Champaign, IL. All soil samples were analyzed for organic matter (% LOI at 600ºC), CEC (Mehlich-3 extraction), pH (1:1 DI water), and buffer pH (Mehlich-3 extraction). For full geochemical processing, pulverized soils were digested using a lithium-borate fusion whereby material was mixed with a lithium meta-borate fluxing agent and heated in a muffle furnace at 1,000 °C to create a molten lithium borate salt. The molten samples were immediately dissolved in a nitric acid solution for characterization *via* inductively coupled plasma (ICP) mass spectrometry (MS) for trace elements (e.g. Ti) and optical emission spectroscopy (OES) for major elements (e.g. Na, Mg, Ca, etc.).

Weathering Rate

The determination of the "weathering rate", or relative proportion of basalt that has dissolved, is a critical aspect of effectively attributing the measured yield effect to the basalt application. Given prolonged timelines of silicate weathering, the heterogenous nature of basaltic feedstocks, and the reliance of weathering on climatic parameters, it is uncertain how much a given basaltic amendment will dissolve within a growing season.

The percent of feedstock dissolution was determined using 2 methods:

1) The total gain in concentration of molar-equivalent (mol-eq/kg soil) base cations (Ca, Mg, Na), delineated as CAT, between BL and R0, or the amount of added average concentration, was compared to the concentration remaining at R3, giving a total percentage of cation loss between R0 and R1.

$$F_{w-FCA} = \frac{(CAT_{R0} - CAT_{R1})}{(CAT_{R0} - CAT_{BL})}$$

2) The shift in cations between R0 and BL is compared to a tau-derived value, where cation values are normalized to Ti shifts prior to comparison:

$$F_{w-Tau} = \left(1 - \frac{\frac{CAT_{R1}}{Ti_{R1}}}{\frac{CAT_{R0}}{Ti_{R0}}}\right) * \frac{CAT_{R0}}{(CAT_{R0} - CAT_{BL})}$$

Field Interpolations

The study area contains 106 time-paired soil samples from three different sampling rounds: baseline (pre-treatment, pre-planting), round 1(post-treatment, pre-soy planting), and round 2 (post-treatment, pre-corn planting). Of the 106 sampling points, 39 are located in the feedstock applied rows and 63 are in non-applied control rows. Sampling points were distributed evenly across the field site in a semi-random schematic.

We used the empirical Bayesian Kriging (EBK) geostatistical interpolation for spatial visualization of soil pH across the field area. EBK was performed for both the baseline and round 2 datasets.

For baseline interpolation, all sample points (n=106) were included, whereas the R2 EBK is two compiled interpolations. The first is for the control points (n=64) and extends to the entire field area, apart from the applied rows. The second was generated independently by using the points in the applied areas and was constrained to the respective boundaries of each row.

Economic Revenue Analysis

To estimate the theoretical increase in per-hectare revenue from the results of this study, we conducted a stochastic Monte Carlo simulation (n=100000), with the corn and soy yield increases set as percentages with the standard error of the mean. There are 3 cost scenarios considered: a) basalt cost, hauling, and application are subsidized between 0-10%, b) basalt cost, hauling, and application are subsidized between 50-60%, and c) basalt cost, hauling, and application are subsidized entirely. These three scenarios are reflective of 3 potential futures in scaled EW deployments: a) soil pH management is a minor component of national agricultural subsidies, b) soil pH management is strong component of national agricultural subsidies, and c) basalt application is either entirely covered by national agricultural subsidies, or farmers are enrolled in programs by EW deployment companies, which all cover the full cost of the amendment for growers. The full list of inputted values used in this simulation can be found in SI Table 1.

To solve for the net revenue gain per-hectare, grower costs of basalt spreading were subtracted from predicted gross increases in profit.

$$\$_{NET} = \$_{GROSS} - \$_{COST}$$

To solve for the gross increase in revenue, the total increase in respective yield was multiplied by potential corn and soy prices with ranges from the past 12 years.

$$\$_{GROSS} = Y_{corn/soy} * Y_{\frac{bushel}{acre}} * \$_{per-bushel}$$

The total cost of spreading was calculated calculating total trucking costs, including material purchase, material hauling and return trips, and fuel efficiency. Application cost per-hectare was also included.

$$\$_{COST} = (app + rock + haul) * (1 - subsidy)$$

$$loads = \frac{app.rate}{subsidy}$$

$$rock = loads_{rock} * cost_{mat}$$

$$haul = 2 * dist. * cost_{truck} * loads$$

References

1. Lamb, W. F. *et al.* The carbon dioxide removal gap. *Nat. Clim. Chang.* **14**, 644–651 (2024).
2. Smith, S. *et al.* The State of Carbon Dioxide Removal 2024 - 2nd Edition. (2024).
3. Beerling, D. J. *et al.* Transforming US agriculture for carbon removal with enhanced weathering. *Nature* 1–10 (2025) doi:10.1038/s41586-024-08429-2.
4. *Climate Change 2022 - Mitigation of Climate Change: Working Group III Contribution to the Sixth Assessment Report of the Intergovernmental Panel on Climate Change*. (Cambridge University Press, 2023). doi:10.1017/9781009157926.
5. Nationally determined contributions under the Paris Agreement. Synthesis report by the secretariat | UNFCCC. https://unfccc.int/documents/650664.
6. Beerling, D. J. *et al.* Challenges and opportunities in scaling enhanced weathering for carbon dioxide removal. *Nat Rev Earth Environ* **6**, 672–686 (2025).
7. Feldhaus, C., Gleue, M., Löschel, A. & Werner, P. The role of co-benefits in motivating climate change mitigation – Experimental evidence. *Ecological Economics* **239**, 108783 (2026).
8. Hultgren, A. *et al.* Impacts of climate change on global agriculture accounting for adaptation. *Nature* **642**, 644–652 (2025).
9. Anwar, M. R., Liu, D. L., Macadam, I. & Kelly, G. Adapting agriculture to climate change: a review. *Theor Appl Climatol* **113**, 225–245 (2013).
10. Xu, C. *et al.* Increasing impacts of extreme droughts on vegetation productivity under climate change. *Nat. Clim. Chang.* **9**, 948–953 (2019).
11. Myers, S. S. *et al.* Climate Change and Global Food Systems: Potential Impacts on Food Security and Undernutrition. *Annu. Rev. Public Health* **38**, 259–277 (2017).
12. Challinor, A. J. *et al.* A meta-analysis of crop yield under climate change and adaptation. *Nature Clim Change* **4**, 287–291 (2014).
13. Rosenzweig, C. *et al.* Assessing agricultural risks of climate change in the 21st century in a global gridded crop model intercomparison. *Proc. Natl. Acad. Sci. U.S.A.* **111**, 3268–3273 (2014).

14. Schlenker, W. & Roberts, M. J. Nonlinear temperature effects indicate severe damages to U.S. crop yields under climate change. *Proc. Natl. Acad. Sci. U.S.A.* **106**, 15594–15598 (2009).

15. Bigelow, D. U.S. Farmland Ownership, Tenure, and Transfer.

16. Bailey, C., Jensen, L. & Ransom, E. Rural America in a Globalizing World.

17. Ranjan, P. *et al.* Understanding barriers and opportunities for adoption of conservation practices on rented farmland in the US. *Land Use Policy* **80**, 214–223 (2019).

18. Carolan, M. S., Mayerfeld, D., Bell, M. M. & Exner, R. Rented land: Barriers to sustainable agriculture. *Journal of Soil and Water Conservation* **59**, 70A-75A (2004).

19. Soule, M. J., Tegene, A. & Wiebe, K. D. Land Tenure and the Adoption of Conservation Practices. *American Journal of Agricultural Economics* **82**, 993–1005 (2000).

20. Wolf, M. K., Wiesmeier, M. & Macholdt, J. Importance of soil fertility for climate-resilient cropping systems: The farmer's perspective. *Soil Security* **13**, 100119 (2023).

21. Crane, T. A., Roncoli, C. & Hoogenboom, G. Adaptation to climate change and climate variability: The importance of understanding agriculture as performance. *NJAS: Wageningen Journal of Life Sciences* **57**, 179–185 (2011).

22. Hartmann, J. *et al.* Enhanced chemical weathering as a geoengineering strategy to reduce atmospheric carbon dioxide, supply nutrients, and mitigate ocean acidification. *Reviews of Geophysics* **51**, 113–149 (2013).

23. Hartmann, J. *et al.* Enhanced chemical weathering as a geoengineering strategy to reduce atmospheric carbon dioxide, supply nutrients, and mitigate ocean acidification. *Reviews of Geophysics* **51**, 113–149 (2013).

24. Pennisi, B. V. Essential pH Management in Greenhouse Crops: pH and Plant Nutrition. *CAES Field Report* https://fieldreport.caes.uga.edu/publications/B1256/essential-ph-management-in-greenhouse-crops-ph-and-plant-nutrition/ (2026).

25. Soil pH, Soil Organic Matter, and Crop Yields in Winter Wheat–Summer Fallow Systems | Agronomy Journal. https://acsess.onlinelibrary.wiley.com/doi/10.2134/agronj2016.08.0462.

26. Jordan, J. S. *et al.* Enhanced rock weathering for improved smallholder farmer welfare: An at-scale case study for rice agriculture in India. *CDRXIV* https://cdrxiv.org/preprint/483 (2026).

27. Beerling, D. J. *et al.* Enhanced weathering in the US Corn Belt delivers carbon removal with agronomic benefits. *Proc Natl Acad Sci U S A* **121**, e2319436121 (2024).

28. Skov, K. *et al.* Initial agronomic benefits of enhanced weathering using basalt: A study of spring oat in a temperate climate. *PLOS ONE* **19**, e0295031 (2024).

29. Vienne, A. *et al.* Enhanced Weathering Using Basalt Rock Powder: Carbon Sequestration, Co-benefits and Risks in a Mesocosm Study With Solanum tuberosum. *Front. Clim.* **4**, (2022).

30. Kelland, M. E. *et al.* Increased yield and CO2 sequestration potential with the C4 cereal Sorghum bicolor cultivated in basaltic rock dust-amended agricultural soil. *Global Change Biology* **26**, 3658–3676 (2020).

31. Pihlap, E. *et al.* Effects of rock amendment on soil physicochemical properties and organic carbon stabilization. *iScience* **28**, 114232 (2025).

32. Liming effects on soil pH and crop yield depend on lime material type, application method and rate, and crop species: a global meta-analysis | Journal of Soils and Sediments | Springer Nature Link. https://link.springer.com/article/10.1007/S11368-018-2120-2.

33. Reershemius, T. *et al.* Initial Validation of a Soil-Based Mass-Balance Approach for Empirical Monitoring of Enhanced Rock Weathering Rates. *Environ. Sci. Technol.* **57**, 19497–19507 (2023).

34. Maxbauer, D. P. *et al.* Evidence for carbon dioxide removal via enhanced rock weathering with steel slag, though not basalt, in a midwestern U.S. field trial. *Front. Clim.* **7**, (2026).

35. Schaffer, Z. R., Rausis, K., Power, I. M. & Paulo, C. Enhanced weathering of kimberlite residues in a field experiment: implications for carbon removal quantification and mine waste valorization. *Front. Clim.* **7**, (2025).

36. Dupla, X., Bertagni, M. B. & Grand, S. Three Years of Field Trials Indicate a Sustained Enhanced Rock Weathering Signal with Limited CO2 Removal. *Environ. Sci. Technol.* **59**, 25751–25764 (2025).

37. te Pas, E. E. E. M., Hagens, M. & Comans, R. N. J. Assessment of the enhanced weathering potential of different silicate minerals to improve soil quality and sequester CO2. *Front. Clim.* **4**, (2023).

38. Soil Acidity and Liming for Agricultural Soils | NC State Extension Publications. https://content.ces.ncsu.edu/soil-acidity-and-liming-for-agricultural-soils.

39. Daniels, R. B. Soil Erosion and Degradation in the Southern Piedmont of the USA.

40. Sherwood, W. C., Hartshorn, A. S. & Eaton, L. S. Soils, geomorphology, landscape evolution, and land use in the Virginia Piedmont and Blue Ridge. in *The Mid-Atlantic Shore to the Appalachian Highlands: Field Trip Guidebook for the 2010 Joint Meeting of the Northeastern and Southeastern GSA Sections* (eds Fleeger, G. M. & Whitmeyer, S. J.) vol. 16 0 (Geological Society of America, 2010).

41. Soil Test Methods From the Southeastern United States.

42. Contrasting soils and landscapes of the Piedmont and Coastal Plain, eastern United States. *Geomorphology* **3**, 417–447 (1990).

43. Chen, F. *et al.* Soil buffering capacity enhances maize yield resilience amidst climate perturbations. *Agricultural Systems* **215**, 103870 (2024).

44. Firth, A. G. *et al.* Dynamics of Soil Organic Carbon and CO2 Flux under Cover Crop and No-Till Management in Soybean Cropping Systems of the Mid-South (USA). *Environments* **9**, 109 (2022).

45. Wagle, P., Gowda, P. H., Anapalli, S. S., Reddy, K. N. & Northup, B. K. Growing season variability in carbon dioxide exchange of irrigated and rainfed soybean in the southern United States. *Science of The Total Environment* **593–594**, 263–273 (2017).

46. Smith, S. F. & Brye, K. R. Carbon Dioxide Emissions as Affected by Alternative Long-Term Irrigation and Tillage Management Practices in the Lower Mississippi River Valley. *The Scientific World Journal* **2014**, 626732 (2014).

47. Pendergrass, A. G., Knutti, R., Lehner, F., Deser, C. & Sanderson, B. M. Precipitation variability increases in a warmer climate. *Sci Rep* **7**, 17966 (2017).

48. Swain, D. L., Langenbrunner, B., Neelin, J. D. & Hall, A. Increasing precipitation volatility in twenty-first-century California. *Nature Clim Change* **8**, 427–433 (2018).
49. Burchfield, E. K., Schumacher, B. L., Spangler, K. & Rissing, A. The State of US Farm Operator Livelihoods. *Front. Sustain. Food Syst.* **5**, (2022).
50. Alternative Fuels Data Center: Maps and Data. https://afdc.energy.gov/data/10338.
51. USDA - National Agricultural Statistics Service Homepage. https://www.nass.usda.gov/.
52. Bureau of Transportation Statistics. National Transportation Statistics (NTS). Preprint at https://doi.org/10.21949/1503663 (2019).

Supplemental Information

Feedstock Characteristics: The basalt used in this field trial is Sunrock Basalt ($Al_{0.41}Fe_{0.11}(Mg_{0.16}Ca_{0.14})Si_{1.17}O_2$), taken from the Butner quarry in Butner, North Carolina. This basalt was analyzed for bulk mineralogy using x-ray diffraction analysis (XRD) (Table 2) and PSD (Figure 4), with a p80 of approximately 89.9 microns (µm), and 37.3% of material below 20 µm. XRD was performed by Activation Laboratories, using the following procedure: Bruker D8 Endeavour diffractometer equipped with Cu X-ray source and operating at the following conditions: 40 kV and 40 mA; range 4-70 deg 2θ for random specimens and 3 – 30 deg 2θ and 3 – 15 deg 2θ for oriented specimens; step size 0.02 deg 2θ; time per step 0.5 sec; fixed divergence slit, angle 0.30; sample rotation 15 rpm. The PDF4/Minerals ICDD database was used for mineral identification. The quantities of the crystalline mineral phases were determined using Rietveld method. The Rietveld method is based on the calculation of the full diffraction pattern from crystal structure data. The relative abundances of clay minerals in the <4µm size fraction were calculated using the relative ratios of their basal-peak areas.

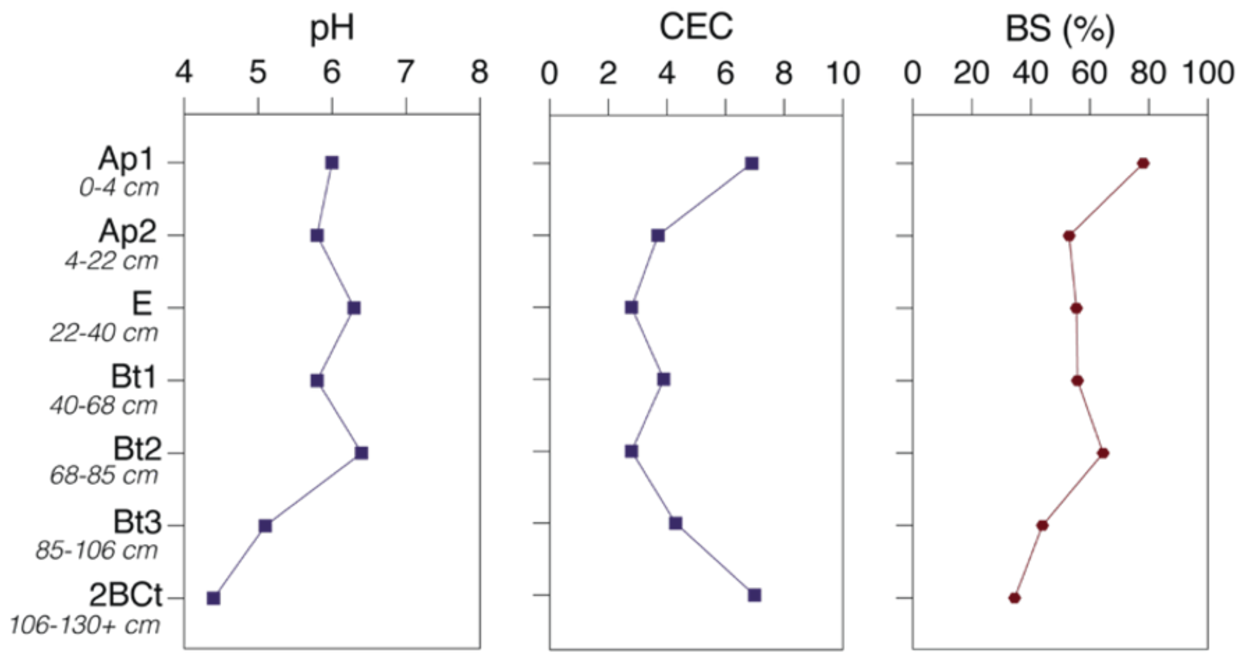

Figure 1. Soil properties and soil profile of presented field. pH was calculated using 1:1 H2O: soil, and cation exchange capacity and base saturation (%) was determined with Melich 3 extraction.

Table 1. Variable Values Used in Monte Carlo Simulations of per-hectare revenue shift

Variable	Description	Units	Value Used	Source	Comment
Y_{corn}	% yield increase in corn	%	[26.67, 46.33]	Empirically derived	
Y_{soy}	% yield increase in soy	%	[7.62, 38.22]	Empirically derived	
app. rate	Application Rate	$t\ ha^{-1}$	49.4	N/A	Application rate used in this trial
dist.	Distance from quarry to farm	km	[20,100]	N/A	Used minimum and maximum values from generalized assumed economic radii
$cost_{mat}$	Material cost	$/t	[0,20]	The Sunrock Group	Assuming range of waste fines to full-price market aggregate product
$\$_{per\text{-}bushel}$	Market price for corn; includes minimum and maximum conventional prices from past 5 years	$\$\ bu^{-1}$, corn	[3.71,8.16]	([50])	
$\$_{per\text{-}bushel}$	Market price for soy; includes minimum and maximum conventional prices from past 10 years	$\$\ bu^{-1}$, soy	[9.53,17.40]	([50])	
$Y_{bushel/hectare}$	Expected theoretical yields for corn	$bu\ ha^{-1}$	[207,518.23]	([51])	Virginia statewide minimum and maximums determined by calculating weighted mean ± 3 weighed σ. Weight determined by acres planted per county.
$Y_{bushel/hectare}$	Expected theoretical yields for soy	$bu\ ha^{-1}$	[58,146]		Virginia statewide minimum and maximums determined by calculating weighted mean ± 3 weighed σ. Weight determined by acres planted per county.
truckload	Maximum hauling per truckload	tons	24	N/A	
$cost_{truck}$	Total cost per ton-kilometer for hauling	$\$\ t^{-1}\ km^{-1}$	[1.354, 3.115]	([52])	

Table 2. Mineralogical abundances of Sunrock basalt from X-ray diffraction analysis (XRD)

Mineral	Abundance (%)
Plagioclase	67.1
Augite/Diopside	13.2
Olivine	4.3
Enstatite, ferroan	5.2
Poorly resolved mineralogy phases	10.9

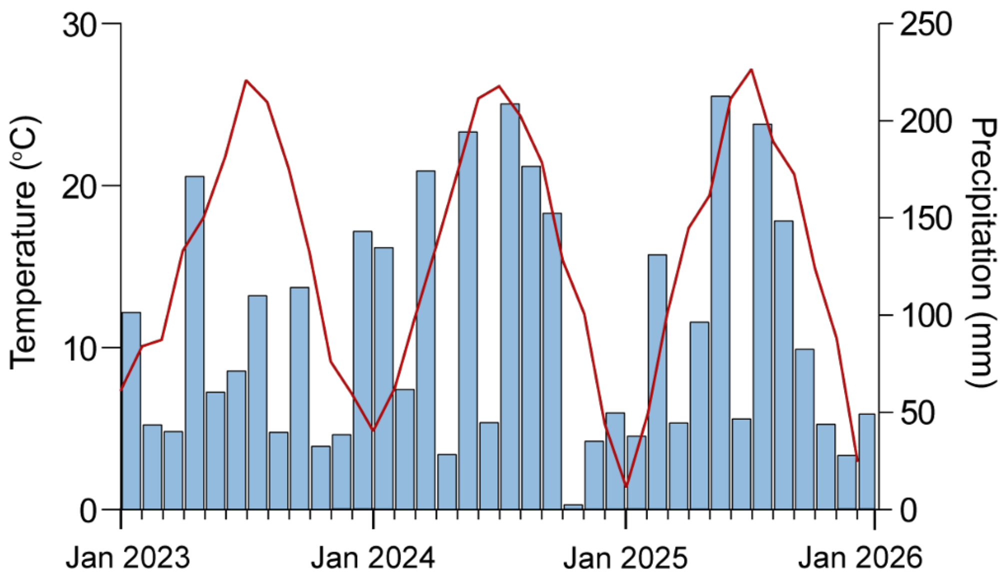

Figure 2. Mean Annual temperature and precipitation in the region between January 2023 and January 2026. Blue bars show cumulative monthly precipitation in mm (right axis), and the red line traces mean annual temperature (left axis). The experimental period represented in this study occurs between May 2024 to August 2025.

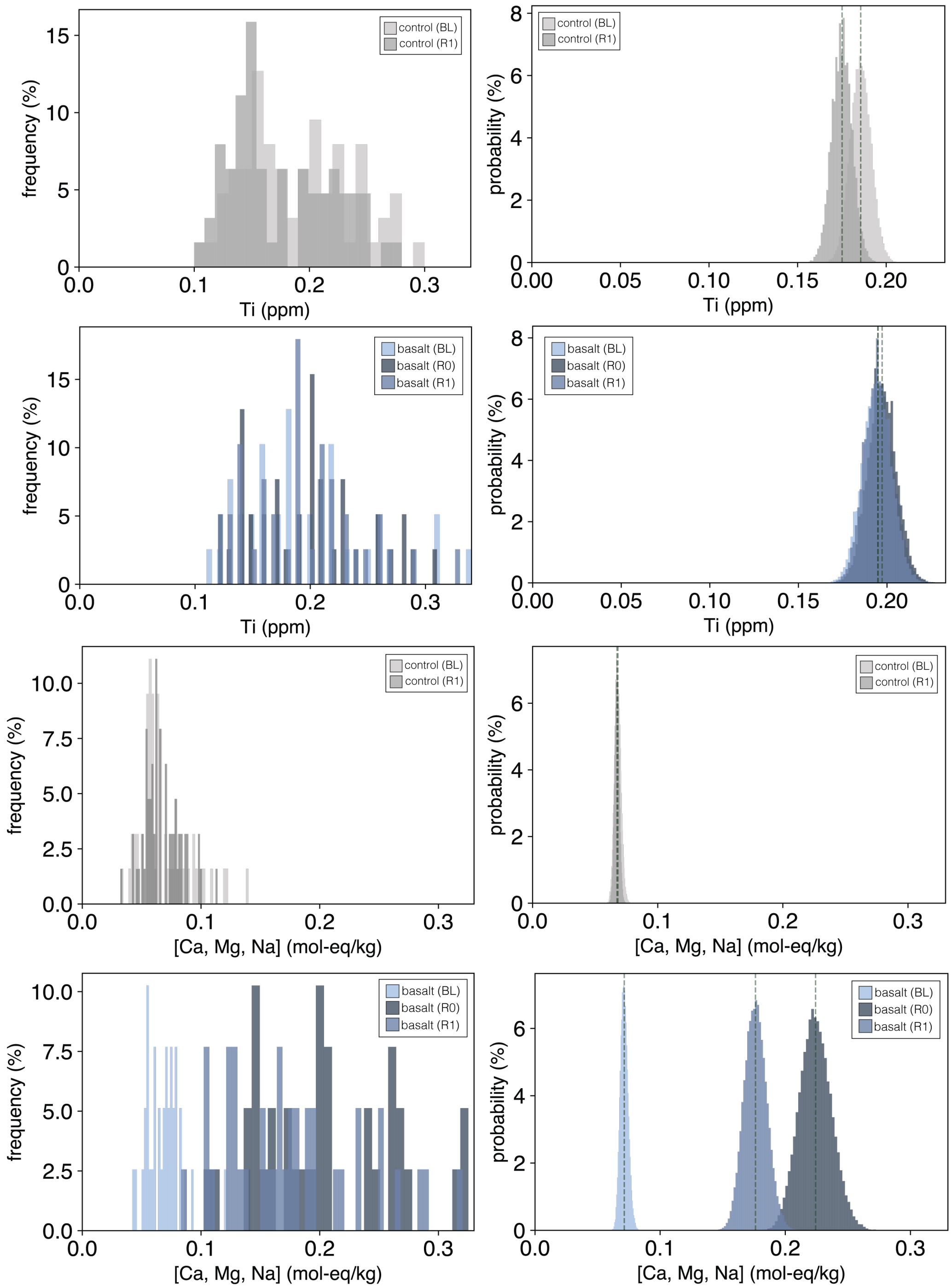

Figure 3. Unbootstrapped and bootstrapped distributions of control and treatment chromium (Cr) concentration in ppm and cation concentration in molar-equivalents per kilogram (kg) of soil. Unbootstrapped concentrations (left panels) show frequency of samples with a given concentration value. Bootstrapped mean concentrations (n=50000 iterations with replacement) show the probability of a mean value within the simulations.

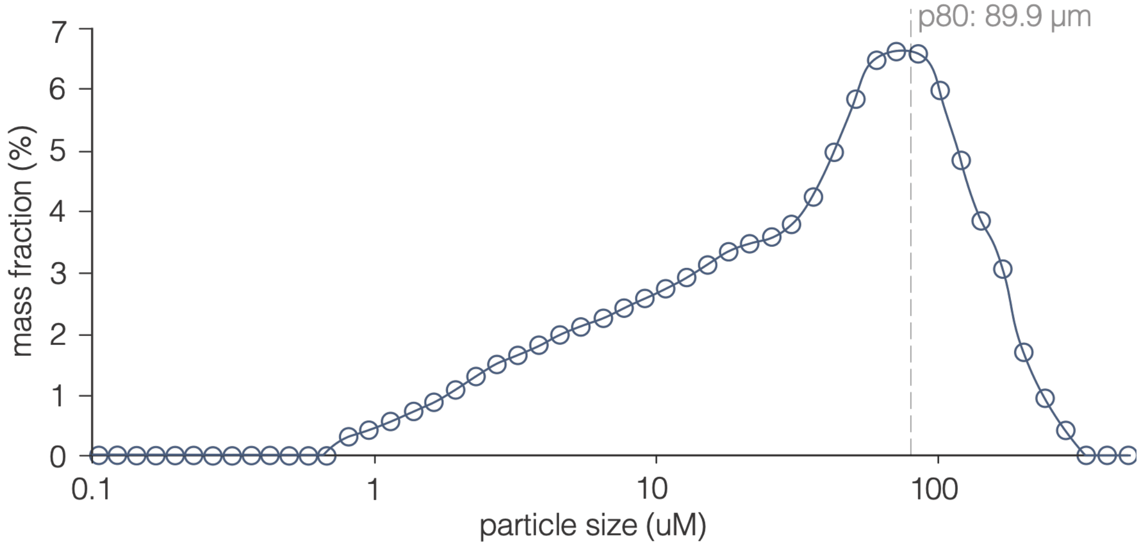

Figure 4. Feedstock particle size distribution of Sunrock basalt used in trial. All analyzed particles were below 250 microns (µm), with a p80 of 89.92 µm. The relative mass fraction of each size bin is shown on the y-axis.